NANO LETTERS

Letter

pubs.acs.org/NanoLett

Quantum-Enhanced Tunable Second-Order Optical Nonlinearity in Bilayer Graphene

Sanfeng Wu,[†] Li Mao,[‡] Aaron M. Jones,[†] Wang Yao,[§] Chuanwei Zhang,[†] and Xiaodong Xu*[,†,∥]

[†]Department of Physics, University of Washington, Seattle, Washington 98195, United States

[‡]Department of Physics and Astronomy, Washington State University, Pullman, Washington, 99164 United States

[§]Department of Physics and Center of Theoretical and Computational Physics, The University of Hong Kong, Hong Kong, China

[∥]Department of Material Science and Engineering, University of Washington, Seattle, Washington 98195, United States

Supporting Information

ABSTRACT: Second order optical nonlinear processes involve the coherent mixing of two electromagnetic waves to generate a new optical frequency, which plays a central role in a variety of applications, such as ultrafast laser systems, rectifiers, modulators, and optical imaging. However, progress is limited in the mid-infrared (MIR) region due to the lack of suitable nonlinear materials. It is desirable to develop a robust system with a strong, electrically tunable second order optical nonlinearity. Here, we demonstrate theoretically that AB-stacked bilayer graphene (BLG) can exhibit a giant and tunable second order nonlinear susceptibility $\chi^{(2)}$ once an in-plane electric field is applied. $\chi^{(2)}$ can be electrically tuned from 0 to ~10^5 pm/V, 3 orders of magnitude larger than the widely used nonlinear crystal $AgGaSe_2$. We show that the unusually large $\chi^{(2)}$ arise from two different quantum enhanced two-photon processes thanks to the unique electronic spectrum of BLG. The tunable electronic bandgap of BLG adds additional tunability on the resonance of $\chi^{(2)}$, which corresponds to a tunable wavelength ranging from ~2.6 to ~3.1 μm for the up-converted photon. Combined with the high electron mobility and optical transparency of the atomically thin BLG, our scheme suggests a new regime of nonlinear photonics based on BLG.

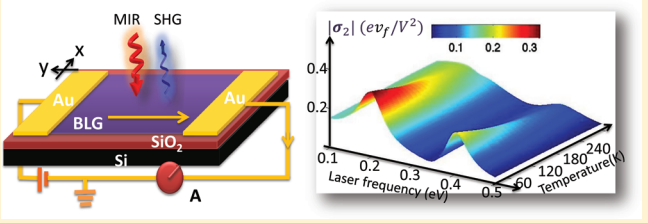

KEYWORDS: *Bilayer graphene, second harmonic generation, double resonance enhancement, perturbation theory, tunability, polarization*

Graphene-based photonics and optoelectronics[1,2] have drawn intense interest because of their combination of unique electronic properties,[3] such as high electron mobility[4] and long mean free path,[5] as well as their excellent optical properties,[1,2,6,7] such as broadband optical absorption[2,6,7] and ultrafast optical response.[8−10] In this context, BLG may have better potential than single layer graphene for photonic applications due to its four-band electronic structure and widely tunable bandgap in the MIR.[11] One promising application is to achieve chip-scale and electrically tunable nonlinear optical devices. Conventional nonlinear optical devices are based on bulk crystals which have poor compatibility with integrated circuits and lack electrical tunability in intensity and wavelength. The required phase matching conditions also lead to volatile signals subject to perturbations from the environment. All these limitations prevent the integration of nonlinear photonics and advanced electronics for new photonic and optoelectronic applications. Here we show that, under realistic device conditions, the difficulties mentioned above can be overcome using the nonlinear optical properties of BLG. Therefore BLG emerges as an excellent $\chi^{(2)}$ material and may provide opportunities for new optoelectronic and photonic applications.

Figure 1a,b shows the atomic structure of BLG and a typical dual-gate field effect transistor (FET) device,[12] respectively. We calculate the intensity of second harmonic generation (SHG)[13−15] following a quantum description of nonlinear optical conductivity. The applied potential bias between top and bottom gates tunes the electronic properties of BLG. The Hamiltonian of BLG near the Dirac points (**K** and **K**′) can be written as[3]

$$H = \sum \psi_{\mathbf{k}}^{\dagger} \mathcal{H}_{\mathbf{k}} \psi_{\mathbf{k}} \tag{1}$$

where

$$\psi_{\mathbf{k}}^{\dagger} = (b_{\mathbf{k}}^{1\dagger}, a_{\mathbf{k}}^{1\dagger}, a_{\mathbf{k}}^{2\dagger}, b_{\mathbf{k}}^{2\dagger})$$

and

$$\mathcal{H}_{\mathbf{k}} = \begin{pmatrix} -\Delta & \hbar v_f g & 0 & 0 \\ \hbar v_f g^* & -\Delta & \gamma_1 & 0 \\ 0 & \gamma_1 & \Delta & \hbar v_f g \\ 0 & 0 & \hbar v_f g^* & \Delta \end{pmatrix}$$

$a_{\mathbf{k}}^{i\dagger}$ ($b_{\mathbf{k}}^{i\dagger}$) is the creation operator for electrons at the sublattice A (B) in the layer $i(i = 1, 2)$, and with momentum in $\mathbf{k}$ the BZ. $\mathbf{k} = (k_x, k_y)$ is the continuous wave vector from **K**,**K**′ and $g = k_x - \xi i k_y$ is a complex number ($\xi = +1$ for **K** and $\xi = -1$ for **K**′).

Received: January 9, 2012
Revised: February 25, 2012
Published: February 28, 2012

ACS Publications © 2012 American Chemical Society

dx.doi.org/10.1021/nl300084j | *Nano Lett.* 2012, 12, 2032−2036

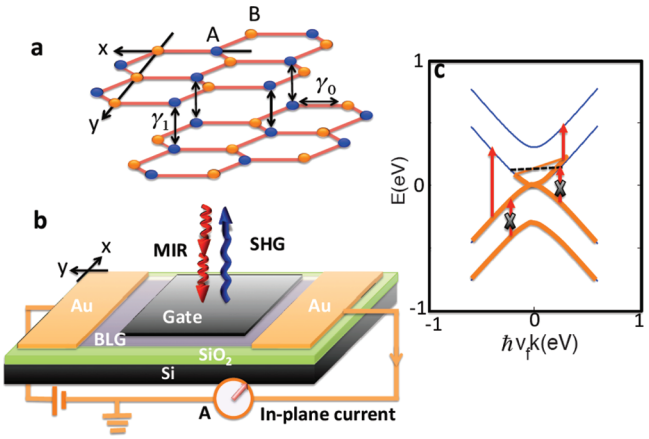

Figure 1. Dual-gated bilayer graphene FET and its optical transitions. (a) Atomic structure of AB-stacked bilayer graphene. γ_1 and γ_0 are the inter- and intralayer hopping parameters. The coordinates used in the calculations are shown. (b) Experimental schematic of using a dual-gated bilayer graphene FET to realize SHG. The in-plane current is set in the $-y$ direction in our calculation. (c) Energy spectrum of BLG and Fermi level shifting when there is an in-plane current between source and drain. Possible and forbidden optical transitions are shown as red arrows. Brown color on the energy levels denotes the occupied states.

The spatial coordinates are defined in Figure 1a,b. $v_f \approx 10^6$ m/s is the Fermi velocity of single layer graphene. Δ ($-\Delta$) describes the potential effect induced by the gate voltages. $\gamma_1 \approx 0.4$ eV is the interlayer hopping parameter.[3] Here we ignore other hopping processes due to their relatively weak strengths. The Hamiltonian (1) has four energy bands, which are obtained by diagonalizing, $\mathcal{H}_k$ and plotted in Figure 1c for $\Delta = 0$.

The total Hamiltonian $\mathcal{H}_p$ that includes the interactions between the BLG and normal incident MIR photons can be obtained by replacing the momentum vector $\hbar\mathbf{k}$ in $\mathcal{H}_k$ with $\mathbf{p} = \hbar\mathbf{k} + e\mathbf{A}$, where $\mathbf{A}$ is the vector potential of the optical fields.[3,16−18] The evolution of the electronic state is determined by the quantum Liouville equation[19]

$$i\hbar\partial_t\rho = [\mathcal{H}_\mathbf{p}, \rho] - i\Gamma(\rho - \rho_{t=0}) \tag{2}$$

where ρ is the time dependent quantum state of electrons with momentum $\mathbf{k}$ at temperature T and chemical potential μ. Γ is a phenomenological parameter for describing the relaxation of electronic states. We $\Gamma = 0.05$ eV set in our calculations,[20] which corresponds to ~80 fs relaxation time of electrons. This is a conservative estimation even at room temperature (The effect of Γ is discussed in Supporting Information[21]). The steady state density matrix in the presence of the optical fields can be obtained by solving the time-dependent eq 2 perturbatively[19] (see Supporting Information[21]).

The optically induced electric current is defined as[22−25]

$$\mathbf{j}_e = \nu e \sum_{BZ} \mathrm{tr}\left(\rho\frac{\partial\mathcal{H}_\mathbf{p}}{\partial\mathbf{p}}\right) = \boldsymbol{\sigma}_1 E e^{i\omega t} + \boldsymbol{\sigma}_2 E^2 e^{i2\omega t} + c.c + \cdots \tag{3}$$

where $\nu = 2$ describes the spin degeneracy and E is the electric field. σ_1 is the linear optical conductivity, which value obtained from our approach is exactly the same as the ones reported using the Kubo formula.[7] Here we focus on the second order nonlinear optical conductivity, which is responsible for SHG. The simplified formula of σ_2^α is[21]

$$\sigma_2^\alpha = \frac{e}{2\pi^2E^2}\int_{BZ}\sum_{ijl}\left[\frac{\rho_\mathbf{k}^{ii} - \rho_\mathbf{k}^{ll}}{\hbar\omega + \varepsilon_i - \varepsilon_l - i\Gamma} - \frac{\rho_\mathbf{k}^{ll} - \rho_\mathbf{k}^{jj}}{\hbar\omega + \varepsilon_l - \varepsilon_j - i\Gamma}\right]\frac{(H_{int})_{il}(H_{int})_{lj}(\eta^\alpha)_{ji}}{2\hbar\omega + \varepsilon_i - \varepsilon_j - i\Gamma}dk \tag{4}$$

where $\alpha = x,y$; $\eta^\alpha = \partial\mathcal{H}_p/\partial\mathbf{p}_\alpha$ $H_{int} = \mathcal{H}_p - \mathcal{H}_k$ is the interaction Hamiltonian and $\rho_k = \mathrm{diag}[f_1, f_2, f_3, f_4]$ is the initial state obtained from the Fermi-Dirac distribution $f_i = 1/\exp[(\varepsilon_i - \mu)/k_BT] + 1$ of electrons at different bands with the band energy $\varepsilon_i (i = 1, 2, 3, 4)$. μ is the chemical potential, k_B is the Boltzmann constant, and T is the temperature.

The above eq 4 has a trivial solution $\sigma_2^\alpha = 0$, although the inversion symmetry of intrinsic BLG (C_{3v} group) has been broken by the vertical biased potential. This is due to the cancellation of the optically excited second order electrical current at opposite momenta ($+\mathbf{k}$ and $-\mathbf{k}$) with respect to both Dirac points. In order to generate a nonzero second order optical nonlinearity, we introduce an in-plane electrical current between source and drain to suppress the cancellation. From semiclassical electron transport theory, the in-plane electric field shifts the Fermi surface by $\Delta\mathbf{k} = m^* u_m j_{dc}/\hbar\sigma_{dc}$ where m^* is the electronic effective mass, j_{sc} is the in-plane current density, σ_{dc} is the DC conductivity, and u_m is the mobility[21] (Figure 1c). According to experimental data of BLG,[1,2,26,27] we take $m^* \approx 0.05m_e$, $u_m \approx 1$ m^2/(V s), $\sigma_{dc} \approx e^2/\hbar$. An energy shift of $\hbar v_f|\Delta\mathbf{k}| \approx 0.01$ eV is achievable with a DC current $j_{dc} \approx 8$ nA/nm. As a result, the Fermi level is shifted (Figure 1c) and the initial electronic state in the presence of j_{sc} turns out to be $\rho_k \leftarrow \rho_{k-\Delta k}$ Physically, due to the Pauli exclusion principle, part of the optical transitions are blocked due to the Fermi level shifting. Therefore the $+\mathbf{k}/-\mathbf{k}$ symmetry is broken and SHG becomes nonzero.

We first explore the second order nonlinear optical conductivity with circularly polarized light excitations. For simplicity, we use left circular polarization as an example. Figure 2a,b plots both the real and imaginary parts of the second order optical conductivity σ_2 at temperatures 30 and 300 K, respectively. σ_2 is decomposed into x and y directions. The induced current at twice the optical frequency has a strong phase-correlation between the x and y directions: $\sigma_2^y = -i\sigma_2^x$. It therefore implies the left circular polarization of the new optical fields generated by SHG is the same as the incident beam. We set the chemical potential $\mu = \gamma_1/2 = 0.2$ eV without the bandgap opening (i.e., $\Delta = 0$). The in-plane electric field is along the y-direction, leading to a shift of $\hbar v_f|\Delta\mathbf{k}| \sim 0.01$ eV. A surprising finding here is the giant enhancement of σ_2 at $\omega = 0.2$ eV and 0.4 eV, as seen from the resonant peaks in Figure 2a,b. The intensities of the resonant peaks increase as the temperature decreases. The ratio of σ_2 at low temperature (30 K) to high temperature (300 K) is about 1.5. In Figure 2c, we plot σ_2 as a function of both temperature and frequency, where these features can be clearly seen.

The two resonant peaks arise from different quantum-enhancement mechanisms. At $\omega = 0.4$ eV, the optical process is dominated by the transitions from the second to the fourth band (2−4 process) and the first to the third band (1−3 process) (Figure 2d) through two-photon absorption. Although two-photon absorption can happen even in BLG in

dx.doi.org/10.1021/nl300084j | Nano Lett. 2012, 12, 2032−2036

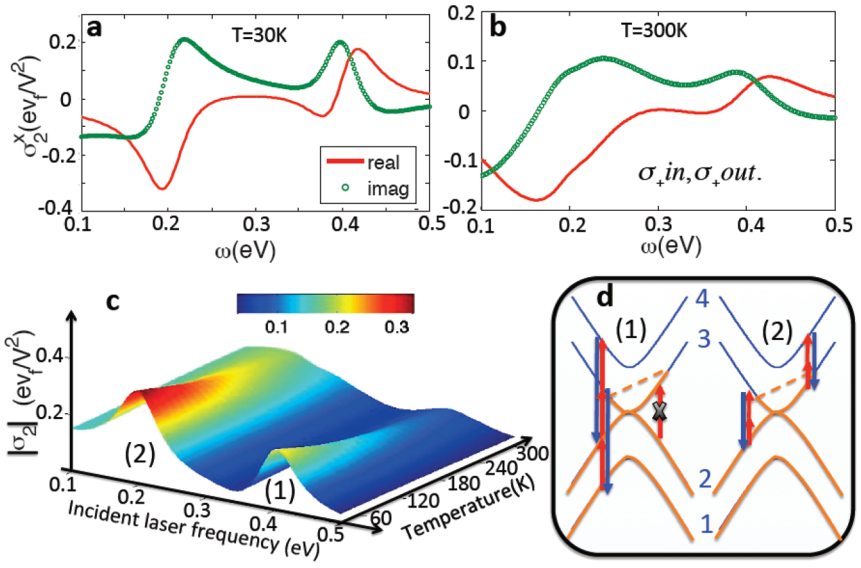

Figure 2. Second order optical response of BLG under left-hand circularly polarized incident laser beam. (a,b) Frequency dependent nonlinear optical conductivity σ_2 calculated at a temperature of 30 and 300 K, respectively. The interlayer hopping parameter γ_1 = 0.4 eV and the phenomenological energy broadening Γ is set to 0.05 eV. Both real and imaginary parts are shown in the x-direction. The response in y-direction can be obtained by $\sigma_2^y = -i\sigma_2^x$. The plots show that there are strongly enhanced responses located at ω = 0.2 and 0.4 eV. (c) σ_2 as a function of temperature and laser frequency. (d) Corresponding optical process for the response peak at (1) ω = 0.4 eV and (2) 0.2 eV.

equilibrium,[28,29] the contributions to SHG from the $\mathbf{K} + \mathbf{k}$ and $\mathbf{K} - \mathbf{k}$ points cancel out. As we mentioned above, the in-plane electric field breaks this symmetry, leading to a shift of the Fermi surface to avoid such cancellation. More importantly, when $\omega = \Delta E_{12} = \Delta E_{23} = \Delta E_{34}$($\Delta E_{ij}$ is the energy difference between the bands i and j), the transient state of SHG is a real state (i.e., the electronic state in the third band or in the second band), giving rise to resonantly enhanced contribution as compared to conventional SHG where the intermediate states are virtual states. In this case, the so-called double resonance-enhanced (DRE) harmonic generation happens in the BLG system. The signal intensity of DRE SHG[30] is usually proportional to $1/\Gamma^2$. We note that the ratio of the contributions between the 1−3 process and 2−4 process is about 1:2 (see Supporting Information).

At ω = 0.2 eV, the contribution to the enhanced signal arises from two different processes, that is, 3−4 and 2−3 (Figure 2d). Both processes have a virtual intermediate state (VIS). In the current situation, the 2−3 process is the leading one, which is responsible for the shift of the peak position at 0.2 eV as T increases to room temperature. The shifting effect arises from the interplay among the temperature T, the Fermi level shifting $\Delta\mathbf{k}$ and the energy band broadening Γ. The shifted amount is about ∼35 meV at room temperature when $\Delta\mathbf{k} \sim 0.01$ eV, $\Gamma \sim 0.05$ eV (see Supporting Information). Clearly, the enhancement of SHG at both and originates from the special band structure of the BLG.

We now explore the second order nonlinear optical conductivity with linearly polarized light excitations. Figure 3 shows σ_2 at the two quantum-enhanced resonant peaks (ω = 0.2 and 0.4 eV) as a function of the incident polarization angle φ with respect to the x-axis. The temperature is set at 180 K. The red solid line denotes the nonlinear response along the x-direction with the blue dashed line along the y-direction. We note that the induced current in the two directions have almost the same phase, which indicates that the output SHG is still linearly polarized. When we vary the incident angle, the optical

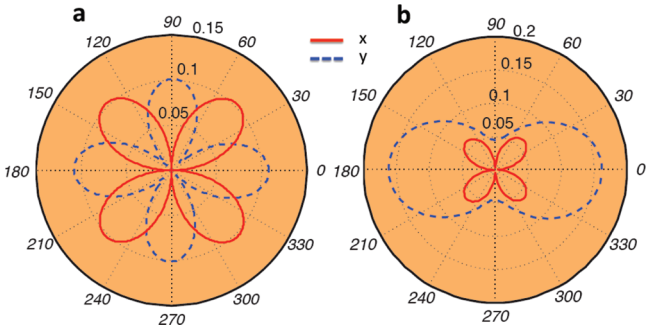

Figure 3. Second order optical response of BLG under linearly polarized incident laser beam. Polar plots of σ_2 versus varying polarization angles of the incident beam starting from the x-axis at T = 180 K for (a) ω = 0.2 eV, and (b) ω = 0.4 eV . The red solid and blue dashed curves correspond to the response in the x- and y-directions, respectively.

conductivities at two different resonant frequencies behave differently. (1) σ_2 enhanced by VIS has a polarization angle $2\varphi + \pi/2$ (Figure 3a). For instance, when the incident laser is polarized at $\varphi = \pi/4$, the second order nonlinear optical conductivity is polarized with angle, that is, in the x-direction. (2) The optical current excited by the DRE mechanism has a preferred axis (y-axis) (Figure 3b). The signal generated in the y-direction (where the in-plane electric field lies) is larger than that in the x-direction. Therefore the output SHG intensity in this situation oscillates around the y-axis as φ varies.

Here we note that the symmetric patterns in Figure 3 do not depend on the relative direction of the in-plane electric fields and lattice orientation. For simplicity, we here set the applied bias along the lattice direction ($-y$), which is not necessary in practice. In general, we find that the second order optical response always behaves in the same way as that shown in Figure 3 for varying directions of the DC current, which determines the symmetric axis of the polar plots (Supporting Information).

dx.doi.org/10.1021/nl300084j | Nano Lett. 2012, 12, 2032−2036

The second order optical susceptibility $\chi^{(2)}$ can be estimated from the optical conductivity[22]

$$\chi^{(2)} = \frac{\sigma_2}{\omega \varepsilon_0 d_{BLG}} \quad (5)$$

Here $d_{BLG} \sim 0.66$ nm is the thickness of BLG and $\varepsilon_0 = 8.85 \times 10^{-12}$ is the vacuum permittivity. Using ev_f/V^2 as a unit for σ_2, we have $\chi^{(2)} \sim 10^5$ pm/V, which is about 3 orders of magnitude larger than state-of-the-art nonlinear crystals in MIR. For comparison, the second order nonlinear susceptibility of the widely used $AgGaSe_2$ crystal is 68 pm/V at a wavelength of ~2.1um.[31] At low temperature and with a large in-plane electric field, the value can be even larger and the response region in our scheme is ultrabroad, as shown below.

We now show that the giant SHG can be tuned by the in-plane electric field, Fermi level, and biased potential Δ. Figure 4a

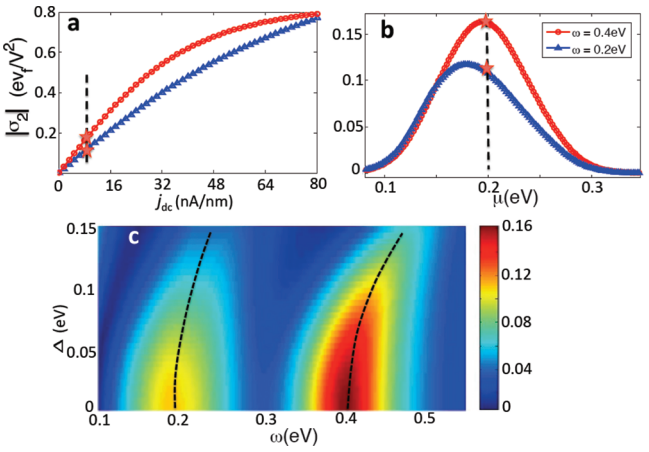

Figure 4. Tunable effects of SHG of BLG. (a) Amplitude of σ_2 as a function of estimated in-plane current (μ = 0.2 eV). (b) Amplitude of σ_2 as a function of Fermi level. μ The red star denotes the value used in our previous calculations. (c) Tunable SHG by controlling the electronic bandgap of BLG. The black dashed lines denote the resonant frequencies. Temperature is set to 180 K.

plots the nonlinear optical conductivity at two resonant peaks as a function of the in-plane current, which is estimated from the shift of the Fermi surface ($\Delta\mathbf{k}$). As an example, the incident laser is set to be polarized in the x-direction and j_{dc} is in the y-direction at a temperature of 180 K. The Fermi level is set to be 0.2 eV. The red stars in the figure represent the parameters we used in the previous discussions in this paper. This plot indicates that SHG intensity increases linearly when the in-plane current is small (<~35 nA/nm), and saturates at high in-plane current. Apparently, if we turn off the in-plane field, SHG is consequently switched off. Unlike conventional electric field-induced SHG that requires an extremely large electric voltage[32] (kilovolts) in the crystal, small in-plane electric fields are more favorable in device applications. In BLG, with an electric field of ~1 V/mm one can electrically switch on and off SHG.

The SHG signal can also be tuned by adjusting the Fermi level, as shown in Figure 4b. Obviously, there is a pronounced SHG when the Fermi level falls in the range around $\gamma_1/2$ = 0.2 eV with Δ = 0. If we increase or decrease the Fermi level without crossing the Dirac point, the effects of the DRE and VIS become less important and the signal decreases to zero. One may notice that the SHG signal will recover when the Fermi level goes down to −0.2 eV (in the p-doping situation).

Finally, we show that the unique bandgap tunability of BLG by an interlayer bias induces the widely tunable resonant frequency of SHG. The intensity plot in Figure 4c shows the magnitude of the second order optical conductivity as a function of Δ and incident laser frequency. In addition to the change of the amplitude of σ_2, an important effect is the variation of the resonant frequency, indicated in Figure 4c by the dashed lines. ω_0 increases from 0.4 to ~0.48 eV for the DRE peak and from 0.2 to ~0.25 eV for the VIS peak, Δ as is tuned from 0 to 0.15 eV. Therefore the resonant wavelengths for SHG are electrically tunable from ~5 to ~6 μm and from ~2.6 to ~3.1 μm. This is another remarkable advantage as compared to conventional nonlinear crystals, where the wavelength for SHG can only be changed by rotating the crystal angles. Moreover, due to its atomic thickness BLG requires no phase matching condition, which is crucial in conventional SHG. Phase matching usually leads to increased sensitivity to environmental perturbations, such as temperature. Therefore, from this point of view SHG of BLG is robust.

In conclusion, we propose a new scheme based on BLG as a nonlinear optical material with an extremely large second order optical susceptibility $\chi^{(2)}$ ~10^5 pm/V. We find that this enhancement arises from two different types of quantum-enhanced mechanisms, unique to the electronic structure of BLG. Our calculation shows an excellent electrical tunability of the optical nonlinearity in both intensity and wavelength compared to conventional nonlinear crystals. Recent experiments show that the nonlinear generation could be detected even through single layer graphene.[14,15,22] The fabrication techniques required here are routine in modern nanotechnology. We expect that our proposal should have a good experimental feasibility. Considering graphene's many unique properties, we believe that our results encourage further experimental investigation toward nonlinear photonics based on BLG and may open new opportunities for graphene applications.

■ ASSOCIATED CONTENT

Supporting Information

Supporting materials include additional information on the calculation of the second order optical conductivity, the effects of electron relaxation time, as well as the in-plane current, and the contributions from different transition processes at both ω = 0.2 eV and ω = 0.4 eV. This material is available free of charge via the Internet at http://pubs.acs.org.

■ AUTHOR INFORMATION

Corresponding Author

*E-mail: xuxd@uw.edu.

Notes

The authors declare no competing financial interest.

■ ACKNOWLEDGMENTS

This work is supported by DARPA YFA N66001-11-1-4124 and NSF-DMR-1150719. L.M. and C.Z. are supported by DARPA-YFA N66001-10-1-4025, DARPA-MTO (FA9550-10-1-0497), and NSF-PHY (1104546). A.J. is supported by NSF Grant DGE-0718124. W.Y. is supported by Research Grant Council of Hong Kong.

■ REFERENCES

(1) Geim, A. K.; Novoselov, K. S. The rise of graphene. *Nat. Mater.* **2007**, *6*, 183−191.

(2) Bonaccorso, F.; Sun, Z.; Hasan, T.; Ferrari, A. C. Graphene photonics and optoelectronics. *Nat. Photonics* **2010**, *4*, 611−622.
(3) Neto, A. H. C.; et al. The electronic properties of graphene. *Rev. Mod. Phys.* **2009**, *81*, 109.
(4) Bolotin, K. I.; et al. Ultrahigh electron mobility in suspended graphene. *Solid State Commun.* **2008**, *146*, 351−355.
(5) Du, X.; Skachko, I.; Barker, A.; Andrei, E. Y. Approaching ballistic transport in suspended graphene. *Nat. Nanotechnol.* **2008**, *3*, 491−495.
(6) Nair, R. R.; et al. Fine Structure Constant Defines Visual Transparency of Graphene. *Science* **2008**, *320*, 1308.
(7) Abergel, D. S. L.; Fal'ko, V. I. Optical and magneto-optical far-infrared properties of bilayer graphene. *Phys. Rev. B* **2007**, *75*, 155430.
(8) Xia, F.; Mueller, T.; Lin, Y.-m.; Valdes-Garcia, A.; Avouris, P. Ultrafast graphene photodetector. *Nat. Nanotechnol.* **2009**, *4*, 839−843.
(9) Mueller, T.; Xia, F.; Avouris, P. Graphene photodetectors for high-speed optical communications. *Nat. Photonics* **2010**, *4*, 297−301.
(10) Sun, D.; Aivazian, G.; Jones, A. M.; Yao, W.; Cobden, D.; Xu, X. Ultrafast Hot-Carrier-Dominated Photocurrent in Graphene. *Nat Nanotechnol.* **2012**, *7*, 114−118; 10.1038nnano.2011.243.
(11) Zhang, Y.; et al. Direct observation of a widely tunable bandgap in bilayer graphene. *Nature* **2009**, *459*, 820−823.
(12) Meric, I.; et al. Current saturation in zero-bandgap, top-gated graphene field-effect transistors. *Nat. Nanotechnol.* **2008**, *3*, 654−659.
(13) Glazov, M. M. Second Harmonics Generation in Graphene. *JETP Lett.* **2011**, *93* (7), 366.
(14) Dean, J. J.; van Driel, H. M. Graphene and few-layer graphite probed by second-harmonic generation: theory and experiment. *Phys. Rev. B* **2010**, *82*, 125411.
(15) Dean, J. J.; van Driel, H. M. Second harmonic generation from graphene and graphitic films. *Appl. Phys. Lett.* **2009**, *95*, 261910.
(16) Mishchenko, E. G. Dynamic Conductivity in Graphene beyond Linear Response. *Phys. Rev. Lett.* **2009**, *103*, 246802.
(17) Mikhailov, S. A. Non-linear electromagnetic response of graphene. *Euro. Phys. Lett.* **2007**, *79*, 27002.
(18) Rosenstein, B.; Lewkowicz, M.; Kao, H. C.; Korniyenko, Y. Ballistic transport in graphene beyond linear response,. *Phys. Rev. B* **2010**, *81*, 041416(R).
(19) (a) Landau, L. D.; Lifshitz, E. M. Quantum Mechanics, Non-Relativistic Theory; Pergamon Press: Oxford, 1977; Vol. 3, p 41. (b) Sakurai, J. J. *Modern Quantum Mechanics*; Addison-Wesley Publishing Company, Inc.: New York, 1994.
(20) Nandkishore, R.; Levitov, L. Polar Kerr Effect and Time Reversal Symmetry Breaking in Bilayer Graphene. *Phys. Rev. Lett.* **2011**, *107*, 097402.
(21) See Supporting Information.
(22) Hendry, E.; et al. Coherent Nonlinear Optical Response of Graphene. *Phys. Rev. Lett.* **2010**, *105*, 097401.
(23) Ang, Y. S.; Sultan, S.; Zhang, C. Nonlinear optical spectrum of bilayer graphene in the terahertz regime. *Appl. Phys. Lett.* **2010**, *97*, 243110.
(24) Lewkowicz, M.; Rosenstein, B. Dynamics of particle-hole pair creation in graphene,. *Phys. Rev. Lett.* **2009**, *102*, 106802.
(25) Dora, B.; Moessner, R. Nonlinear electric transport in graphene: Quantum quench dynamics and the Schwinger mechanism. *Phys. Rev. B* **2010**, *81*, 165431.
(26) Zhang, L. M.; et al. Determination of the electronic structure of bilayer graphene from infrared spectroscopy. *Phys. Rev. B* **2008**, *78*, 235408.
(27) Zou, K.; et al. Effective mass of electrons and holes in bilayer graphene: Electron-hole asymmetry and electron-electron interaction. *Phys. Rev. B* **2011**, *84*, 085408.
(28) Yang, H.; Feng, X.; Wang, Q.; Huang, H.; Wei Chen, W.; Wee, A. T. S.; Ji, W. Giant Two-Photon Absorption in Bilayer Graphene. *Nano Lett.* **2011**, *11* (7), 2622−2627.
(29) Lim, G.; Chen, Z.; et al. Giant broadband nonlinear optical absorption response in dispersed graphene single sheets. *Nat. Photonics* **2011**, *5*, 554−560.
(30) Rosencher, E.; Bois, P. Model system for optical nonlinearities: Asymmetric quantum wells. *Phys. Rev. B* **1991**, *44*, 11315−11327.
(31) Chung, I.; et al. Helical Polymer $1/\infty[P_2Se_6^{2-}]$: Strong Second Harmonic Generation Response and Phase-Change Properties of Its K and Rb Salts. *J. Am. Chem. Soc.* **2007**, *129*, 14996−15006.
(32) Hakuta, K.; Marmet, L.; Stoicheff, B. P. Electric-field-induced second-harmonic generation with reduced absorption in atomic hydrogen. *Phys. Rev. Lett.* **1991**, *66*, 596−599.